Structural forms of single crystal semiconductor nanoribbons for high-performance stretchable electronics

Yugang Sun*[a] and John A. Rogers*[b]

Received 11th October 2006, Accepted 11th January 2007
First published as an Advance Article on the web 25th January 2007
DOI: 10.1039/b614793c

This feature article reviews some concepts for forming single-crystalline semiconductor nanoribbons in 'stretchable' geometrical configurations with emphasis on the materials and surface chemistries used in their fabrication and the mechanics of their response to applied strains. As implemented with ribbons that have periodic or aperiodic sinusoidal 'wavy' or 'buckled' shapes and are surface chemically bonded to elastomeric poly(dimethylsiloxane) (PDMS) supports, these concepts enable levels of mechanical stretchability (and compressibility) that exceed, by orders of magnitude, the intrinsic fracture strains in the ribbon materials themselves. These results, in combination with active functional device elements that can be formed on the surfaces of these 'wavy' or 'buckled' ribbons, represent a class of potentially valuable building blocks for stretchable electronics, with application possibilities in personal or structural health monitors, sensory skins, spherically curved focal plane arrays and other systems that cannot be achieved easily with other approaches.

1. Introduction

The vast majority of research and development work in electronics for the last half century has focused on reducing the dimensions of individual functional devices to increase circuit operating speeds and integration densities and to reduce the overall sizes of end applications. A different direction, which emerged in the last couple of decades, seeks to enlarge, rather than shrink, the area coverage of the electronics and to enable such systems to be formed on cheap, non-wafer based substrates, such as glass or plastic, for applications where traditional wafer scale electronics is not suitable. This type of large-area electronics are most useful for home theater display systems, but they also have a wide range of other potential applications, especially when formed on lightweight flexible supports, such as paperlike displays and optical scanners,[1–3] conformable sensory skins for robotic sensors,[4,5] conformal X-ray imagers[6] and others. Thin film transistors (TFTs) fabricated with flexible semiconductors, such as amorphous and polycrystalline thin films and arrays or networks of nanowires, nanotubes and nanoribbons,[7–16] on large-area plastic sheets have the potential to serve as active building blocks for these types of applications. Some impressive demonstration devices in the area of flexible displays have been achieved.[2,17,18] One limitation of this type of electronics is that their bendability only enables them to be rolled into cylindrical or conical shapes with moderate bend radii ($\sim$1 cm is typical). These devices cannot be wrapped around a sphere, as a means to form a hemispherical curve focal plane array for a wide viewing angle camera, or onto a complex curvilinear surface like the wing of an aircraft, as a means to create a sensory surface for structural health monitoring. The type of fully reversible mechanical response that includes both bendability and stretchability represents a characteristic that is much more challenging than just bendability, because all known semiconductor materials fracture at strains larger than a few percent. One strategy that avoids this problem combines rigid device islands that are interconnected by stretchable conductors such as structured films of gold, doped elastomers, coiled wires and others.[19–26] Electronics that use this construction are promising, especially for applications in electronic textiles and other devices that involve relatively low coverage of active electronics.[27,28] This feature article reviews a different strategy, in which the circuit level stretchability originates directly from stretchability not only in the interconnects but also in the active device elements themselves, through the use of nanoribbons of high-quality, single-crystal inorganic semiconductor materials that are formed in engineered geometrical configurations and are surface chemically bonded to elastomeric poly(dimethylsiloxane) (PDMS) substrates. Integrating such stretchable semiconductor nanoribbons with dielectrics, patterns of dopants, and thin metal films can generate high-performance, stretchable electronic devices. The general approaches for fabricating stretchable nanoribbons with an emphasis on the materials and surface chemical aspects, and representative examples of stretchable electronic devices are discussed.

2. Stretchable structures

Perhaps the most intuitive configuration of a ribbon that enables stretchability is a coil, or helix, similar to a telephone cord as illustrated in Fig. 1a. Such a helix behaves

[a]*Center for Nanoscale Materials, Argonne National Laboratory, 9700 South Cass Avenue, Argonne, Illinois, 60439, USA. E-mail: ygsun@anl.gov; Fax: (+1) 630-252-4646*
[b]*Department of Materials Science and Engineering, Department of Chemistry, Beckman Institute and Frederick Seitz Materials Research Laboratory, University of Illinois at Urbana-Champaign, Urbana, Illinois, 61801, USA. E-mail: jrogers@uiuc.edu; Fax: (+1) 217-244-2278*

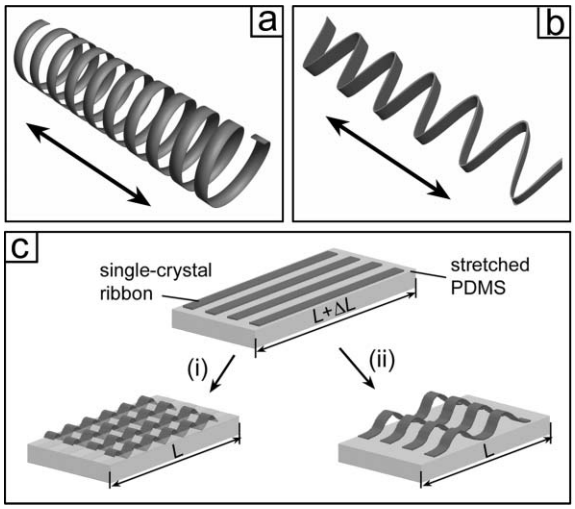

Fig. 1 Semiconductor ribbons with (a) spiral and (b) rippled configurations exhibit mechanical stretchability. (c) Schematic illustration of procedures for fabricating rippled semiconductor nanoribbons on elastomeric PDMS substrates. Wavy and buckled profiles on PDMS surfaces that are functionalized for surface chemical bonding uniformly along the lengths of the ribbons (step i) and selectively along only certain portions of the ribbons (step ii).

mechanically like spring, according to Hooke's law, $F = k \times \Delta x$, where F is the force applied to stretch the ribbon along the helix axis (as indicated by the double-arrowed line), k is a constant determined by the material of the ribbon and the geometric parameters of the helix, and Δx is the change in the length of the helix. Helices of semiconductor nanoribbons can be fabricated by starting with strained multilayered films grown on single-crystal wafers,[29–31] lithographically cutting them into ribbon shapes, and then releasing them from their supporting substrates by dissolving the substrates or sacrificial layers underneath the ribbons. Upon release, the strained layers in the ribbons cause them spontaneously to bend upward and roll into tubes[32–37] or helices.[29–31] The thickness, composition, and longitudinal crystalline orientation of the ribbons as well as the shape of the mesa of the etched substrates determine the geometries (tubes *versus* helices) and physical parameters (*e.g.*, diameter, *etc.*) of the resulting structures. The strong correlation between the geometry of the helices and properties of materials in the stacks can, in some cases, limit the ability to control the shapes for desired applications. Helices of several kinds of semiconductor materials can also grow through chemical synthetic approaches,[38–40] but such structures, in most cases, have modest properties in terms of geometrical uniformity, compositional controllability, *etc.* compared with the helices fabricated from wafers. Free-standing helices formed using either of these methods can be difficult to integrate into architectures for functional applications due to their fragility and their coiled layouts. A different geometry that also provides stretchability involves rippled structures, similar to those reported for stretchable thin gold films (or stripes) deposited on PDMS stamps,[19–26,41] as illustrated in Fig. 1b. The rippled structure acts like an 'accordion bellows'; it stores relatively low energy when the period and amplitudes of the waves are large compared to the thickness of the ribbons. All of these dimensions can be controlled in the fabrication process, as described in the following. As typically fabricated from unstrained, flat ribbons, the tensile/compressive strains reach their maximum values on the surfaces of the ribbons at the peaks and troughs of the waves. Ribbons with this geometry can be surface chemically bonded to an elastomeric substrate that can provide a restoring force for reversible response upon stretching/compressing. In this case, the substrate, which has a Young's

Yugang Sun

Yugang Sun received B.S. and Ph.D. degrees in chemistry from the University of Science and Technology of China (USTC) in 1996 and 2001, respectively. From 2001 to 2006, he was a research associate at the University of Washington and University of Illinois at Urbana-Champaign. He is currently an assistant scientist for the Center for Nanoscale Materials in Argonne National Laboratory. His research interests include synthesis and characterization of nanostructures, micro/nanofabrication, nanobiotechnology, and devices for optics and electronics. He has published more than 60 journal papers and a number of book chapters.

John A. Rogers

John A. Rogers obtained B.A. and B.S. degrees in chemistry and in physics from the University of Texas, Austin, in 1989. From MIT, he received S.M. degrees in physics and in chemistry in 1992 and a Ph.D. degree in physical chemistry in 1995. From 1995 to 1997, Rogers was a Junior Fellow in the Harvard University Society of Fellows. During this time he also served as a Director for Active Impulse Systems, a company based on his Ph.D. research that he co-founded in 1995 and which was acquired by a large company in 1998. He joined Bell Laboratories as a Member of Technical Staff in the Condensed Matter Physics Research Department in 1997, and served as Director of this department from 2000 to 2002. He is currently Founder Professor of Engineering at University of Illinois at Urbana/Champaign, with appointments in the Departments of Materials Science and Engineering, Electrical and Computer Engineering, Mechanical Science and Engineering and Chemistry. Rogers' research includes fundamental and applied aspects of nano- and molecular scale fabrication, materials and patterning techniques for large area electronics and unusual photonic systems. He has won many awards for this work, which is published in more than 150 papers and ~60 patents, more than half of which are licensed or in active use.

modulus (*i.e.*, ~2 MPa) that is nearly five orders of magnitude smaller than those of typical single-crystalline semiconductors (*e.g.*, 130 GPa for Si and 85.5 GPa for GaAs), serves both as a support and an element that configures the ribbons into their 'wavy' (and 'buckled') geometries. The control enabled by the fabrication process allows straightforward formation and integration of functional devices with desired levels of stretchability and bendability for envisioned applications. This feature article highlights the approaches for fabricating such types of stretchable semiconductors, their mechanical behaviors and integration into high-performance electronic devices including field effect transistors, diodes and photodetectors.

3. Surface chemistry of PDMS and semiconductor nanoribbons

PDMS is composed of polymeric chains constructed with repeating units of $-(CH_3)_2SiO_2-$. Scheme 1 shows the molecular configuration (top left). The high density of methyl groups ($-CH_3$) at the surface leads to the hydrophobicity of the pristine PDMS surface. This property combined with the low Young's modulus and low surface energy enables the formation of conformal contact, through the action of generalized adhesion forces (*e.g.*, van der Waals force in most cases), between a flat piece of PDMS with almost any substrate (the top part of Scheme 1) that has sufficient smoothness. In general, this kind of force is very weak, on the order of hundreds of times lower than a typical chemical bond (*e.g.*, Si–O).[42–44] Oxidizing the PDMS surface by exposure to ozone, for example, produces a surface that can react with a wide range of materials such as ceramics, oxides, *etc.* to form strong chemical bonds, simply upon physical contact at room or slightly elevated temperatures. The enhanced reactivity is attributed to the conversion of the hydrophobic surface to a strongly hydrophilic state due to the formation of surface silanol groups (–Si–OH), generated from the oxidation of $-CH_3$ on the surface of PDMS.[45,46] Oxygen plasma and ultraviolet (UV) light exposure represent the most explored approaches to oxidize PDMS due to the efficiency with which they generate highly active oxygen species, such as O_2^+, O_2^-, O for oxygen plasma[47] and O_3 for UV exposure.[45,48] These oxygen species can attack the Si atoms (as indicated by the blue arrow) in the surface chains to remove the methyl groups, resulting in the formation of polar silanol groups. The precise mechanisms associated with these oxidation reactions are not clearly understood, but the results of surface analysis obtained by X-ray photoluminescence spectroscopy (XPS), attenuated total reflection infrared (ATR-IR) spectroscopy and static secondary ion mass spectroscopy (SSIMS) confirm the consumption of $-CH_3$ and the formation of –Si–OH during oxidation.[45,46] The left part (gray background) of Scheme 1 lists the possible surface groups on the oxidized PDMS. Prolonged oxidization, achieved through high concentration of oxygen species and/or long oxidation times, can reduce the reactivity of the surface due to the formation of stable SiO_2 network-like structures along with a decrease of density of silanol groups and an increase in the modulus of the near surface layer in a manner that can frustrate conformal contact. In the following procedures, the oxidation is accomplished through relatively short time exposures of bulk pieces of PDMS to UV induced ozone (UVO), due to the simplicity of the processing equipment and the ease with which the oxidation conditions can be controlled.

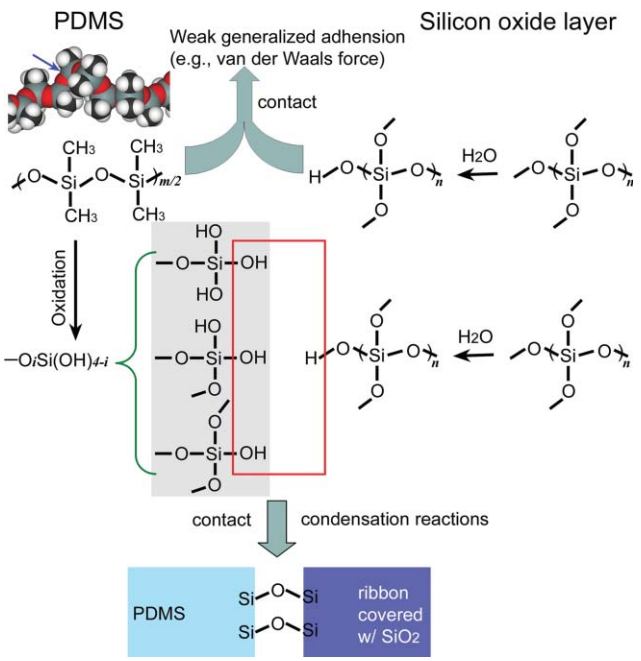

Scheme 1 Illustration of the surface chemistry of PDMS and reactions occurring at the interfaces between PDMS and semiconductor nanoribbons covered with thin SiO_2 layers.

Surface chemical contact bonding is critically important for the fabrication of stretchable semiconductor nanoribbons, as described below. Although oxidized PDMS (with high density of silanol groups) can form bonds with various surfaces,[46] we selected SiO_2 as the bonding layer on the ribbons because of its electrically insulating character and the very strong bonding that exhibits to PDMS upon contact even at room temperature. For this purpose, a thin layer of SiO_2 is either deposited or grown on the surfaces of the as-fabricated ribbons. Water in the ambient atmosphere might be able to diffuse into the SiO_2 to interact with the lattice vacancies on its surface to form silanol groups (as shown in the right part of Scheme 1).[49,50] When oxidized PDMS contacts such a SiO_2 layer, strong covalent chemical bonds, *i.e.*, siloxane bonds (–Si–O–Si–), form between the PDMS stamp and the SiO_2 through condensation reactions (as indicated in the red box) at room temperature or as accelerated during baking at elevated temperatures (*e.g.* 50–100 °C).[45] These chemical bonds are strong enough that attempts to remove ribbons from the PDMS result in cohesive mechanical failure in the PDMS rather than adhesive failure at the ribbon/PDMS interface. Without the oxidation steps, ribbons bond to the PDMS only through weak van der Waals interactions, and can be reversibly attached or detached. This ability to modulate the adhesion, through lithographic patterning of the PDMS surface chemistry, provides the basis for fabricating a wide range of rippled structures in the nanoribbons.

4. Wavy nanoribbons

Fig. 1c depicts two strategies for preparing semiconductor nanoribbons with different geometries on PDMS substrates. The first step in both cases involves fabricating semiconductor nanoribbons from a source wafer (referred to as *mother wafer*) by patterning and chemical etching using 'top-down' approaches, according to procedures described elsewhere.[51–56] The anchors at the ends of the ribbons keep them attached to the mother wafer even after they have been completely undercut etched along their lengths. This procedure allows the ribbons to retain the order defined by the lithographic methods used in their fabrication. These steps can be adapted for a wide range of material classes, although most of our work on stretchable ribbons focuses on Si and GaAs structures fabricated from silicon-on-insulator (SOI) wafers and GaAs/AlAs/GaAs wafers, respectively.[57–59] In the case of GaAs, electron-beam evaporation of SiO_2 forms the thin film adhesive coating. The native oxide layers play the same role in the case of Si. In the next step, laminating a pre-stretched PDMS substrate (*e.g.*, from a length of L to $L + \Delta L$, resulting in a prestrain of $\varepsilon_{pre} = \Delta L/L$, the top frame of Fig. 1c) with an oxidized surface onto the ribbons leads to the formation of conformal contact between the ribbons and PDMS. In the cases shown here, the ribbons lie along the direction of prestrain. Van der Waals and/or surface chemical bonding between the ribbons and PDMS are sufficiently strong that peeling the PDMS from the mother wafer transfers all the ribbons to the surface of the PDMS.[51,56] Relaxing the pre-stretched PDMS transforms the ribbons into rippled geometries with layouts that are determined by the level of prestrain, the mechanical properties of the PDMS and the ribbons, the widths, lengths and thicknesses of the ribbons, and the type and pattern of bonding sites on the PDMS.

As a simple example, PDMS substrates that bond strongly along the entire lengths of the ribbons lead to highly sinusoidal, wavy structures (step i, Fig. 1c).[57,58] Fig. 2 shows examples of such structures formed with GaAs ribbons (thickness of 270 nm and width of 100 μm) covered with a 2 nm Ti/28 nm SiO_2 bilayer. Frames a, b, and c of Fig. 2 show images collected with an optical microscope, scanning electron microscope (SEM) and atomic force microscope (AFM), respectively, from the same sample, *i.e.*, wavy GaAs ribbons formed with prestrain of ~1.9% (created by thermal expansion of the PDMS at 90 °C). The images clearly show the formation of periodic, wavy structures in the GaAs ribbons. The inset of Fig. 2a presents a diffraction pattern formed by passing a laser beam oriented perpendicular to the surface of PDMS through the wavy ribbons; the regular pattern of diffracted spots confirms the periodic nature of these structures. Linecuts (Fig. 2d) through the AFM images (Fig. 2c) provide a quantitative measure of the geometries. The contour (blue curve) parallel to the longitudinal direction (*i.e.*, as indicated by the double arrowed line) of the ribbon clearly shows a periodic, wavy profile, consistent with a computed fit to a sine wave (dashed line of Fig. 2d). The wavy geometry is quantitatively consistent with an approximate nonlinear analysis of the rippled geometry in a uniform, thin, high-modulus layer on a semi-infinite low-modulus support.[41,60] The dependence of the vertical displacement

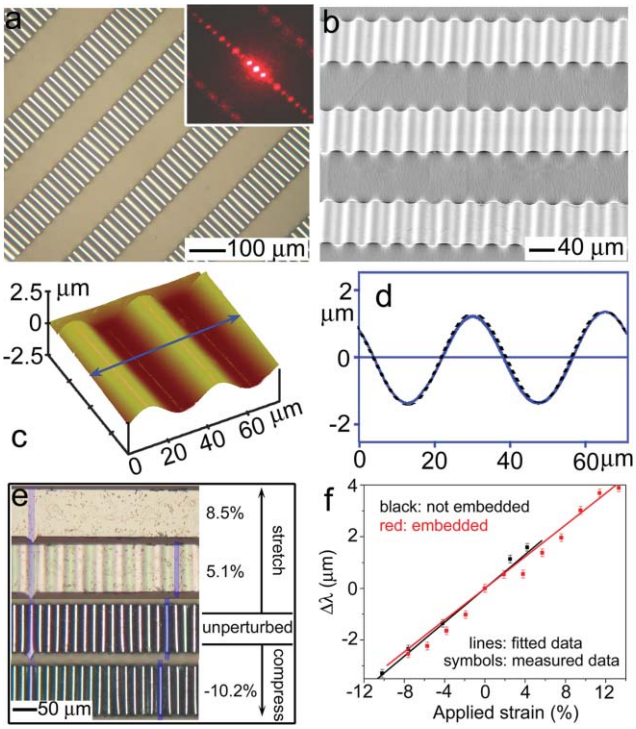

Fig. 2 Characterization of wavy GaAs nanoribbons with thicknesses of 270 nm and widths of 100 μm and coated with a bilayer of 2 nm Ti/28 nm SiO_2. (a) Optical microscope, (b) SEM and (c) AFM images of wavy ribbons formed on a PDMS substrate pre-stretched by 1.9%. (d) Line cut (solid, blue) from the AFM image (c) along an individual ribbon, showing the periodic, sinusoidal profile, consistent with the calculated result (dotted black line). (e) Optical micrographs of wavy GaAs ribbons formed with a prestrain of 7.8% recorded at different applied strains. The blue bars on the left and right highlight certain peaks in the structure; the variation in the distance between these bars indicates the dependence of the wavelength on applied strain. (f) Change in wavelength as a function of applied strain for the wavy GaAs ribbons shown in (e), plotted in black; similar data for a system of sample (e) embedded in PDMS, plotted in red.

(y_{wavy}) of each wave on the position (x) in the plane of the PDMS surface follows:

$$y_{wavy} = A_{wavy,0}\sin\left(\frac{2\pi}{\lambda_{wavy,0}}x\right)$$
$$\text{with } \lambda_{wavy,0} = \frac{\pi h}{\sqrt{\varepsilon_c}},\ A_{wavy,0} = h\sqrt{\frac{\varepsilon_{pre}}{\varepsilon_c} - 1} \quad (1)$$

where $\varepsilon_c = 0.52\left[\frac{E_{PDMS}(1-\nu_{ribbon}^2)}{E_{ribbon}(1-\nu_{PDMS}^2)}\right]^{2/3}$ is the critical strain for buckling, ε_{pre} is prestrain, $\lambda_{wavy,0}$ and $A_{wavy,0}$ are the wavelength and amplitude of the resulting waves, respectively. The Poisson ratio is ν, the Young's modulus is E, and the subscripts refer to properties of the ribbons or PDMS. h represents the thickness of the ribbons. As indicated in eqn (1), the wavelength and amplitude of the waves are proportional to the thickness of ribbons when the prestrain is constant. The peak-to-peak amplitude and wavelength associated with this function are 2.56 and 35.0 μm, respectively, for the sample shown in Fig. 2a–c. The strains determined from the ratio of the horizontal distances between the adjacent two peaks on the stamp (*i.e.*, the wavelength) to the contour lengths between

these two points (*i.e.*, the surface distances measured by AFM) are referred to as *ribbon strains*. The values for the sample shown in Fig. 2a–c are ~1.3%, which is smaller than the prestrain (1.9%) for pre-stretching the PDMS. This difference might originate from two possibilities: *i*) low modulus of PDMS and *ii*) island effects related to the length of GaAs ribbons being shorter than the length of PDMS substrate.[61] The tensile strains at the surfaces of the ribbons in the regions of the peaks in the waves (referred to *peak strains*) are approximately given by the bending strains in those locations: $\varepsilon_{\text{wavy}}^{\text{peak}} = \frac{2\pi^2 A_{\text{wavy},0} h}{\lambda_{\text{wavy},0}^2}$ The peak strains in the ribbons of Fig. 2a–c are ~0.62%, consistent with bending strains inferred from the curvatures determined by AFM. The peak strain is more than a factor of 2 smaller than the ribbon strain (*i.e.*, 1.3%). This mechanical advantage provides stretchability in the GaAs ribbons, with physics similar to that in wavy nanoribbons of other materials, *e.g.*, Si.[57] The prestrain can be increased up to ~15% to generate wavy structures with peak strains that remain lower than the yield point (~2%) for GaAs. The second bottom frame of Fig. 2e shows an image of a wavy GaAs ribbon formed with a prestrain of ~7.8%.

The dynamic response of the wavy structures to tensile and compressive strains applied to the elastomeric substrate is critical for stretchable electronic devices. The stretchability and compressibility of wavy ribbons are determined by the change in the length of the substrate (which is referred to applied strain, $\varepsilon_{\text{applied}}$) parallel to the longitudinal dimension of the ribbons. The wavelengths (λ_{wavy}) and amplitudes (A_{wavy}) of the wavy ribbons vary with applied strains in a manner that is in full agreement with rigorous finite element modeling of the system. In particular, these parameters change with applied strain according to the following approximate relations:

$$\begin{aligned} \lambda_{\text{wavy}} &= \lambda_{\text{wavy},0}\left(1+\varepsilon_{\text{applied}}\right) \\ A_{\text{wavy}} &= \sqrt{A_{\text{wavy},0}^2 - h^2\frac{\varepsilon_{\text{applied}}}{\varepsilon_c}} = h\sqrt{\frac{\varepsilon_{\text{pre}}-\varepsilon_{\text{applied}}}{\varepsilon_c}-1} \end{aligned} \quad (2)$$

where $\varepsilon_{\text{applied}}$ is positive for stretching and negative for compressing. Fig. 2e shows a series of photographs of a wavy GaAs ribbon under different applied strains. The measured linear dependence of wavelength change on the applied strains appears in Fig. 2f (black symbols). In practical applications, encapsulating the ribbons (and devices built with them) in a way that maintains their stretchability can be beneficial. A simple approach is to cast and cure PDMS pre-polymers on samples such as the one shown in Fig. 2e to embed the wavy ribbons in a homogeneous, electrically inert PDMS matrix. The resulting encapsulated systems exhibit similar mechanical behavior to the unembedded ones, *i.e.*, stretching increases wavelength and compressing decreases wavelength (the red lines and symbols in Fig. 2f). Experimental results indicate that wavy ribbons generated with a prestrain of ~7.8% can be stretched or compressed to strains of up to ~10% without inducing any observable fractures in the GaAs.

5. Buckled nanoribbons

On pre-stretched PDMS substrates where the surface is oxidized only in selected areas, the semiconductor ribbons form buckled structures that involve complete separations of the ribbons from the PDMS in the unoxidized regions (step ii, Fig. 1c). As an example, consider a PDMS substrate pre-stretched by 60% and patterned with a UVO mask,[45,59] to define parallel, surface activated (oxidized) narrow stripes (widths, W_{act}, of 10 μm) separated by wide, unactivated regions (widths, W_{in}, of 400 μm) of pristine surface. Contacting such a PDMS substrate with preformed ribbons on the mother wafer, as before, removing the substrate and then relaxing its prestrain leads to large buckled structures forming in the ribbons, the geometries of which are controlled by strong surface chemical bonding at the activated sites and weak bonding in the other regions (inset of Fig. 3a). Fig. 3a shows an SEM image of buckled GaAs ribbons (with thickness and width of 270 nm and 100 μm, respectively, and covered with a 30 nm thick layer of SiO_2) formed on such a PDMS substrate. The image reveals uniform, periodic buckles with common geometries and spatially coherent phases for all ribbons in the array. The anchoring points are well registered on the stamp to the adhesion sites defined by the UVO mask. The width of the adhesion sites is ~10 μm, consistent with W_{act}. The bottom frame of Fig. 3b presents a side-view optical photograph clearly showing the separation of GaAs ribbon from the PDMS in the buckled regions. The vertical displacements associated with these buckles (measured relative to the flat surface of the PDMS stamp) can be written as

$$y = \frac{1}{2}A_{\text{buckled},0}\left(1+\cos\frac{\pi}{L_0^1}x\right) \quad (3)$$

where $A_{\text{buckled},0} = \frac{4}{\pi}\sqrt{L_0^1 L_0^2\left(\varepsilon_{\text{pre}} - \frac{h^2\pi^2}{12L_0^1L_0^1}\right)}$, and $L_0^1 = \frac{W_{\text{in}}}{2\times\left(1+\varepsilon_{\text{pre}}\right)}$, $L_0^2 = L_0^1 + \frac{W_{\text{act}}}{2}$. The profiles calculated according to eqn (3), plotted as dotted red lines, agree well with observations in GaAs ribbons (Fig. 3b). The buckle width ($L_{\text{buckled},0}$) of the initial buckles is $2L_0^1$ and the periodicity is $2L_0^2$. Because $\frac{h^2\pi^2}{12L_0^1L_0^1}$ is much smaller than ε_{pre} (*i.e.*, >10% in most cases) for $h < 1$ μm, the amplitude can be simplified as $\frac{4}{\pi}\sqrt{L_0^1L_0^2\varepsilon_{\text{pre}}}$, which is independent of the properties of ribbons (*e.g.*, thickness, chemical composition, Young's modulus, *etc.*). Therefore, the geometries of buckles are mainly determined by the layout of UVO masks and the prestrains in PDMS substrates. This conclusion suggests a general applicability of this approach and controllability over the parameters of buckles by tuning the fabrication processes. The maximum tensile strain (*i.e.*, *peak strain*) in the buckled ribbons is, approximately, $\varepsilon_{\text{buckled}}^{\text{peak}} = \frac{h}{4}A_{\text{buckled},0}\left(\frac{\pi}{L_0^1}\right)^2$. The peak strain for this sample is only 0.61%, which is ~100 times smaller than the ε_{pre}. This mechanical advantage is significantly larger than that possible with the wavy geometry described in the previous section.

The width of the buckles can be tuned by controlling the prestrains and/or the value of W_{in}.[59] For high levels of stretchability, it is beneficial for ε_{pre} to be as high as possible with appropriately selected values of W_{in} and W_{act}. Fig. 3b shows a series of side-view photographs of buckled GaAs ribbons, all with ε_{pre} = 60% and W_{act} = 10 μm, but with different W_{in}. The profiles agree well with analytical solutions

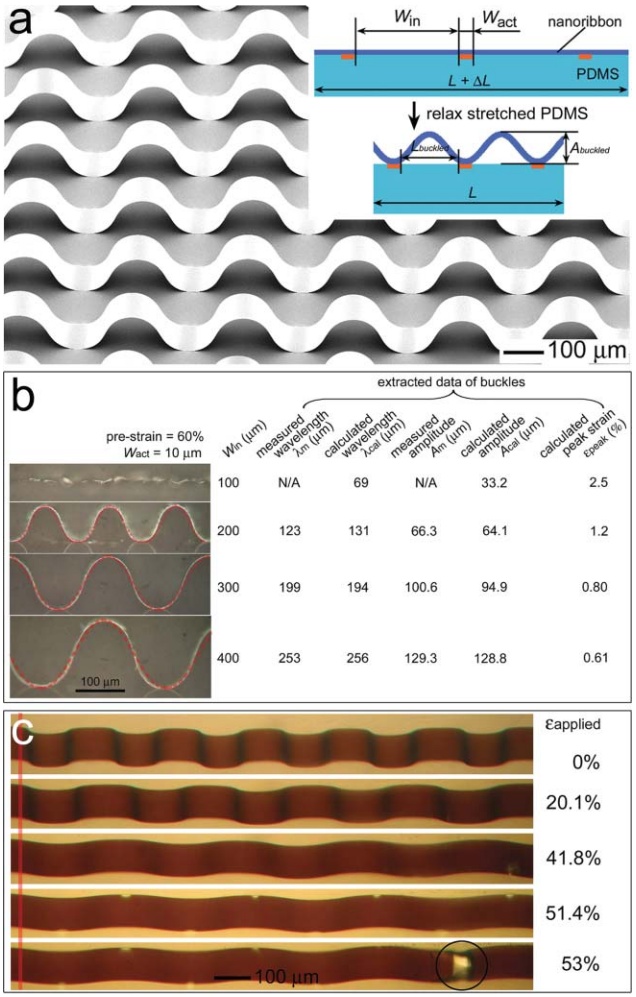

Fig. 3 Characterization of buckled GaAs ribbons with thicknesses of 270 nm and widths of 100 μm and covered with a 30 nm thick layer of SiO_2. (a) SEM image of a sample formed on a PDMS substrate that was pre-stretched by 60% and patterned with W_{act} = 10 μm and W_{in} = 400 μm. The image was recorded by tilting the sample at an angle of 38°. (b) Buckled structures formed on PDMS substrates pre-stretched to 60% with W_{act} = 10 μm and different W_{in}: 100, 200, 300, and 400 μm (from top to bottom). (c) Optical micrographs of a single buckled ribbon (embedded in PDMS matrix) stretched to different levels of tensile strain. Cracking failure, highlighted by the circle, occurs near 53%. The buckles in the ribbon were formed with prestrain of 60% and W_{act} = 10 μm, W_{in} = 400 μm. The red line indicates the same position on this ribbon.

to the mechanics (dashed red lines) except for the sample formed with W_{in} = 100 μm. The cracking failures in the ribbons that occur when W_{in} = 100 μm (and smaller) results from tensile strains (~2.5% in this case) that exceed the yield point of the GaAs (~2%). Therefore, it is important to pattern PDMS stamps with $W_{in} \gg W_{act}$. The parameters extracted from observations and calculations are consistent, as indicated in Fig. 3b. An important feature of this approach is that the lithographically defined adhesion sites can have any geometries, in particular those that are more complex than the simple grating patterns associated with the structures in Fig. 3. Typical examples include arrays of ribbons where buckles with different widths and amplitudes form in individual ribbons, and those where buckles form with different phases for different ribbons.[59]

The dynamic response of the buckled ribbons to stretching and compressing is mainly accommodated by changes in the shapes of the buckles. Under stretching or compressing, widths ($L_{buckled}$) and heights ($A_{buckled}$) vary with applied strains according to:

$$L_{buckled} = 2L^1_{buckled}$$

and

$$A_{buckled} = \frac{4}{\pi}\sqrt{L^1_{buckled}L^2_{buckled}\left(\varepsilon_{pre} - \varepsilon_{applied} - \frac{h^2\pi^2}{12L^1_{buckled}L^1_{buckled}}\right)} \quad (4)$$

where $L^1_{buckled} = \frac{W_{in}}{2\times(1+\varepsilon_{pre}-\varepsilon_{applied})}$ and $L^2_{buckled} = L^1_{buckled} + \frac{W_{act}}{2}$. As predicted from eqn (4), upon stretching, the heights of buckles decrease and the widths increase; in contrast, the heights of buckles increase and the widths decrease during compression. Buckled ribbons can be stretched to a level of strain that approaches ε_{pre}, which can be as high as 100%. Similar to the wavy ribbons, the buckled systems can also be embedded in PDMS without significant effect on their stretchability. Fig. 3c shows a series of optical images of a buckled GaAs ribbon embedded in PDMS when stretched to different strains. Here, the initial buckles involved a prestrain of 60% with a PDMS substrate patterned with W_{in} = 400 μm and W_{act} = 10 μm. As shown in the images, the ribbon can be stretched up to ~51.4% without failure. In addition, the buckled ribbons in this case can also be compressed as high as ~18.7% without breaking. These data show clearly the high levels of stretchability and compressibility that can be achieved from buckled semiconductor ribbons by optimizing the fabrication processes.

6. Stretchable electronics

In addition to active semiconductors, other materials (*e.g.*, metal layers for electrodes, dielectric layers, *etc.*) for functional devices can be integrated with nanoribbons similar to those described in the previous sections, before or after transfer to PDMS. For example, stretchable metal-oxide-semiconductor field-effect transistors (MOSFETs) (with geometry sketched in Fig. 4a) made of wavy Si ribbons (thickness of 2.5 μm and width of 50 μm) can be fabricated using approaches described in section 4, where the device fabrication is performed on the mother wafer prior to transfer onto PDMS.[57] The resulting devices exhibit wavy morphologies as shown in the middle frame of Fig. 4b (MOSFET). This figure also shows images of the device under different levels of applied strain. The device does not show significant changes (<20% for saturation current) in electrical properties (Fig. 4c) even when it is stretched and compressed up to 9.9%, and it works well even after hundreds of cycles of compressing/stretching. This kind of stretchable transistor exhibits high carrier mobilities, *i.e.*, ~100 $cm^2\ V^{-1}\ s^{-1}$. In addition, p–n diodes can also be fabricated by doping the Si ribbons with boron and phosphorus before their formation and transfer to PDMS. The diodes could be used as photodetectors (at reverse-biased

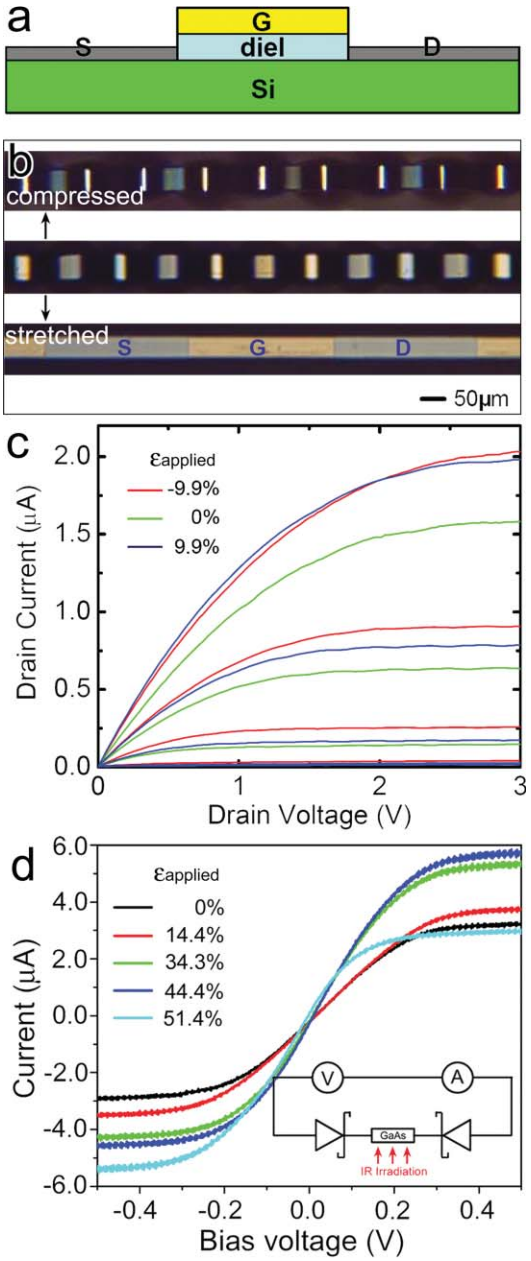

Fig. 4 (a) Geometry, (b) optical images and (c) electrical characteristics of a stretchable Si ribbon MOSFET on a PDMS substrate stretched at different levels. The golden and bluish-gray regions in the ribbon correspond to gate (G, formed with 2 nm Cr/25 nm Au bilayer) and source (S)/drain (D) (formed with 25 nm Cr layers) regions, respectively. The oxide layer (SiO_2) was thermally grown on the ribbon. Gate length of the transistor was 500 μm. The transistor was fabricated through the so-called self-alignment process. (d) Electrical properties of a stretchable GaAs-ribbon MSM photodetector recorded under illumination of an infrared light source (wavelength of 850 nm) and with different stretching strains. The inset is the equivalent circuit of the photodetector. The electrodes are made of a 30 nm thick Au layer. GaAs ribbons used in the photodetectors have thickness of 270 nm and width of 100 μm, and a surface covered with a 30 nm thick SiO_2 layer. The buckled geometry formed in the ribbons is similar to that shown in Fig. 3a. The part of the buckled ribbon between two electrodes is embedded in the PDMS matrix. Frames a, b and c provided courtesy of D.-Y. Khang.

state) or as photovoltaic devices, in addition to their use as normal rectifying devices.

Semiconductor ribbons with large buckled geometries (shown in Fig. 3) can also be used to fabricate stretchable electronics. Fig. 4d shows, for example, the electrical characteristics of a stretchable metal–semiconductor–metal (MSM) photodetector formed with a buckled GaAs ribbon. Here, the buckles have geometries similar to the structures shown in Fig. 3a and c, and are embedded in PDMS. The inset shows the equivalent circuit. Current flow through the photodetector increases with the illumination of an infrared beam (wavelength of ~850 nm), as expected. Fig. 4d shows a series of current–voltage (I–V) curves recorded at different applied strains. The current increases for stretching up to 44.4% and then decreases with further stretching. The increases in current with stretching can be attributed to increases in the projected area of the buckled GaAs ribbon as it flattens. Because the intensity per unit area of the light source is constant, the number of photons received by the photodetector increases during stretching. Further stretching the photodetector might induce the formation of defects on the surface and/or in the lattice of the GaAs ribbon, resulting in the decrease of current. When the photodetector is stretched beyond a critical level, it fractures to form an open circuit, resulting in no current. This device can also work well even when it is compressed by 18%. These results indicate that buckled GaAs ribbons embedded in PDMS matrix provide a fully stretchable/compressible type of photosensor that could find applications in various areas including wearable monitors, curved imaging arrays and other devices.

7. Conclusion

Due to their low modulus, highly elastic behavior up to large strains, excellent physical toughness and, most important, tailorable surface chemistry, PDMS sheets provide a unique type of substrate for forming stretchable electronics based on wavy and buckled structures of thin semiconductor ribbons. Approaches that involve the transfer of nanoribbons from wafer sources are particularly attractive because they naturally allow device and circuit processing to occur on the wafer, rather than on the dimensionally unstable PDMS. The static and dynamic mechanical behaviors of these unusual combinations of materials can be fully accounted for by analytical and finite element modeling of the systems. Future research might include the development of reliable techniques for large-area fabrication as well as integration of elemental electronic units into functional circuits for systems level applications. In addition to electronics, stretchable sensing devices of different types might be possible using the approaches described here when implemented with previously reported non-stretchable nanoribbons that provide various sensing capabilities.[62–70] The integration of such stretchable sensors with stretchable electronics can yield important applications. For example, stretchable photodetectors (as shown in Fig. 4d) formed with the use of photo-sensitive nanoribbons integrated with stretchable electronic circuits could yield artificial eyes or hemispherical curve focal plane arrays for wide viewing angle cameras. Integration of the stretchable electronic circuits with

sensors for pressure, temperature, various chemical and biological species onto surgical gloves may represent a new and important class of medical device. These and other possibilities suggest that stretchable (compressible) electronics could find immediate applications in many envisioned areas requiring mechanical characteristics that are difficult or impossible to achieve with conventional substrates (*e.g.* Si, glass, *etc.*) or even emerging materials such as flexible plastic sheets. Realistic embodiments of such devices will require not only the sensors and electronics but also the packaging materials. We demonstrated that PDMS can be used to encapsulate wavy/buckled semiconductor nanoribbons in a manner that maintains their stretchability/compressibility (Fig. 3c). The chemical instability of PDMS in severe conditions,[71] however, must be considered for realistic applications. Considerations such as these indicate clearly that materials research will continue to play a central role in this newly emerging field of electronics.

Acknowledgements

The work was supported by the U.S. Department of Energy under Grant No. DEFG02-91-ER45439. Argonne National Laboratory's work (for Y. Sun) was supported by the U.S. Department of Energy, Office of Science, Office of Basic Energy Sciences, under contract DE-AC02-06CH11357. The authors thank Dr Dahl-Young Khang for providing images and characterization data for stretchable Si devices.

References

1 J. A. Rogers, Z. Bao, K. Baldwin, A. Dodabalapur, B. Crone, V. R. Raju, V. Kuck, H. Katz, K. Amundson, J. Ewing and P. Drzaic, *Proc. Natl. Acad. Sci. U. S. A.*, 2001, **98**, 4835.
2 G. H. Gelinck, H. E. A. Huitema, E. Van Veenendaal, E. Cantatore, L. Schrijnemakers, J. B. P. H. Van Der Putter, T. C. T. Geuns, M. Beenhakkers, J. B. Giesbers, B.-H. Huisman, E. J. Meijer, E. M. Benito, F. J. Touwslager, A. W. Marsman, B. J. E. Van Rens and D. M. De Leeuw, *Nat. Mater.*, 2004, **3**, 106.
3 T. Someya, Y. Kato, S. Iba, Y. Noguchi, T. Sekitani, H. Kawaguchi and T. Sakurai, *IEEE Trans. Electron Devices*, 2005, **52**, 2502.
4 T. Someya, T. Sekitani, S. Iba, Y. Kato, H. Kawaguchi and T. Sakurai, *Proc. Natl. Acad. Sci. U. S. A.*, 2004, **101**, 9966.
5 T. Someya, Y. Kato, T. Sekitani, S. Iba, Y. Noguchi, Y. Murase, H. Kawaguchi and T. Sakurai, *Proc. Natl. Acad. Sci. U. S. A.*, 2005, **102**, 12321.
6 A. Nathan, B. Park, A. Sazonov, S. Tao, I. Chan, P. Servati, K. Karim, T. Charania, D. Striakhilev, Q. Ma and R. V. R. Murthy, *Microelectron. J.*, 2000, **31**, 883.
7 R. H. Reuss, B. R. Chalamala, A. Moussessian, M. G. Kane, A. Kumar, D. C. Zhang, J. A. Rogers, M. Hatalis, D. Temple, G. Moddel, B. J. Eliasson, M. J. Estes, J. Kunze, E. S. Handy, E. S. Harmon, D. B. Salzman, J. M. Woodall, M. A. Alam, J. Y. Murthy, S. C. Jacobsen, M. Olivier, D. Markus, P. M. Campbell and E. Snow, *Proc. IEEE*, 2005, **93**, 1239.
8 P. C. van der Wilt, M. G. Kane, A. B. Limanov, A. H. Firester, L. Goodman, J. Lee, J. R. Abelson, A. M. Chitu and J. S. Im, *MRS Bull.*, 2006, **31**, 461.
9 Q. Cao, S.-H. Hur, Z.-T. Zhu, Y. Sun, C. Wang, M. A. Meitl, M. Shim and J. A. Rogers, *Adv. Mater.*, 2006, **18**, 304.
10 G. Grüner, *J. Mater. Chem.*, 2006, **16**, 3533.
11 X. Duan, C. Niu, V. Sahi, J. Chen, J. W. Parce, S. Empedocles and J. Goldman, *Science*, 2003, **425**, 274.
12 E. Menard, K. J. Lee, D.-Y. Khang, R. G. Nuzzo and J. A. Rogers, *Appl. Phys. Lett.*, 2004, **84**, 5398.
13 Z.-T. Zhu, E. Menard, K. Hurley, R. G. Nuzzo and J. A. Rogers, *Appl. Phys. Lett.*, 2005, **86**, 133507.
14 J.-H. Ahn, H.-S. Kim, K. J. Lee, Z. Zhu, E. Menard, R. G. Nuzzo and J. A. Rogers, *IEEE Electron Device Lett.*, 2006, **27**, 460.
15 Y. Sun, S. Kim, I. Adesida and J. A. Rogers, *Appl. Phys. Lett.*, 2005, **87**, 083501.
16 Y. Sun, E. Menard, J. A. Rogers, H.-S. Kim, S. Kim, G. Chen, I. Adesida, R. Dettmer, R. Cortez and A. Tewksbury, *Appl. Phys. Lett.*, 2006, **88**, 183509.
17 R. A. Street, W. S. Wong, S. E. Ready, M. L. Chabinyc, A. C. Arias, S. Limb, A. Salleo and R. Lujan, *Mater. Today*, 2006, **9**(4), 32.
18 J. Jang, *Mater. Today*, 2006, **9**(4), 46.
19 J. Jones, S. P. Lacour, S. Wagner and Z. Suo, *J. Vac. Sci. Technol., A*, 2004, **22**, 1723.
20 T. Li, Z. Huang, Z. Suo, S. P. Lacour and S. Wagner, *Appl. Phys. Lett.*, 2004, **85**, 3435.
21 S. P. Lacour, J. Jones, S. Wagner, T. Li and Z. Suo, *Proc. IEEE*, 2005, **93**, 1459.
22 S. P. Lacour, D. Chan, S. Wagner, T. Li and Z. Suo, *Appl. Phys. Lett.*, 2006, **88**, 204103.
23 Z. Y. Huang, W. Hong and Z. Suo, *J. Mech. Phys. Solids*, 2005, **53**, 2101.
24 S. P. Lacour, C. Tsay and S. Wagner, *IEEE Electron Device Lett.*, 2004, **25**, 792.
25 T. Li and Z. Suo, *Int. J. Solids Struct.*, 2006, **43**, 2351.
26 D. S. Gray, J. Tien and C. S. Chen, *Adv. Mater.*, 2004, **16**, 393.
27 E. Bonderover and S. Wagner, *IEEE Electron Device Lett.*, 2004, **25**, 295.
28 T. Li, Z. Y. Huang, Z. C. Xi, S. P. Lacour, S. Wagner and Z. Suo, *Mech. Mater.*, 2005, **37**, 261.
29 L. Zhang, E. Ruh, D. Grützmacher, L. Dong, D. J. Bell, B. J. Nelson and C. Schönenberger, *Nano Lett.*, 2006, **6**, 1311.
30 L. Zhang, E. Deckhardt, A. Weber, C. Schönenberger and D. Grützmacher, *Nanotechnology*, 2005, **16**, 655.
31 V. Ya. Prinz, V. A. Seleznev, A. K. Gutakovsky, A. V. Chehovskiy, V. V. Preobrazhenskii, M. A. Putyato and T. A. Gavrilova, *Physica E*, 2000, **6**, 828.
32 O. G. Schmidt and K. Eberl, *Nature*, 2001, **410**, 168.
33 Ch. Deneke and O. G. Schmidt, *Appl. Phys. Lett.*, 2004, **85**, 2914.
34 R. Songmuang, N. Y. Jin-Phillipp, S. Mendach and O. G. Schmidt, *Appl. Phys. Lett.*, 2006, **88**, 021913.
35 S. V. Golod, V. Ya. Prinz, P. Wägli, L. Zhang, O. Kirfel, E. Deckhardt, F. Glaus, C. David and D. Grützmacher, *Appl. Phys. Lett.*, 2004, **84**, 3391.
36 V. Seleznev, H. Yamaguchi, Y. Hirayama and V. Prinz, *Jpn. J. Appl. Phys., Part 2*, 2003, **42**(7A), L791.
37 V. Ya. Prinz, V. A. Seleznev, V. A. Samoylov and A. K. Gutakovsky, *Microelectron. Eng.*, 1996, **30**, 439.
38 H.-F. Zhang, C.-M. Wang and L.-S. Wang, *Nano Lett.*, 2002, **2**, 941.
39 X. Y. Kong, Y. Ding, R. Yang and Z. L. Wang, *Science*, 2004, **303**, 1348.
40 P. X. Gao, W. Mai and Z. L. Wang, *Nano Lett.*, 2006, **6**, 2536.
41 N. Bowden, S. Brittain, A. G. Evans, J. W. Hutchinson and G. M. Whitesides, *Nature*, 1998, **393**, 146.
42 Y. Y. Huang, W. Zhou, K. J. Hsia, E. Menard, J.-U. Park, J. A. Rogers and A. G. Alleyne, *Langmuir*, 2005, **21**, 8058.
43 K. J. Hsia, Y. Huang, E. Menard, J.-U. Park, W. Zhou, J. Rogers and J. M. Fulton, *Appl. Phys. Lett.*, 2005, **86**, 154106.
44 W. Zhou, Y. Huang, E. Menard, N. R. Aluru, J. A. Rogers and A. G. Alleyne, *Appl. Phys. Lett.*, 2005, **87**, 251925.
45 W. R. Childs, M. J. Motala, K. J. Lee and R. G. Nuzzo, *Langmuir*, 2005, **21**, 10096.
46 D. C. Duffy, J. C. McDonald, O. J. A. Schueller and G. M. Whitesides, *Anal. Chem.*, 1998, **70**, 4974.
47 P. F. Kurunczi, J. Guha and V. M. Donnelly, *Phys. Rev. Lett.*, 2006, **96**, 018306.
48 W. R. Childs and R. G. Nuzzo, *J. Am. Chem. Soc.*, 2002, **124**, 13583.
49 T. Bakos, S. N. Rashkeev and S. T. Pantelides, *Phys. Rev. Lett.*, 2002, **88**, 055508.
50 R. H. Doremus, *J. Mater. Res.*, 1995, **10**, 2379.
51 Y. Sun and J. A. Rogers, *Nano Lett.*, 2004, **4**, 1953.

52 Y. Sun, D.-Y. Khang, F. Hua, K. Hurley, R. G. Nuzzo and J. A. Rogers, *Adv. Funct. Mater.*, 2005, **15**, 30.
53 Y. Sun, R. A. Graff, M. S. Strano and J. A. Rogers, *Small*, 2005, **1**, 1052.
54 S. Mack, M. A. Meitl, A. J. Baca, Z.-T. Zhu and J. A. Rogers, *Appl. Phys. Lett.*, 2006, **88**, 213101.
55 H. C. Ko, A. J. Baca and J. A. Rogers, *Nano Lett.*, 2006, **6**, 2318.
56 K. J. Lee, M. J. Motala, M. A. Meitl, W. R. Childs, E. Menard, A. K. Shim, J. A. Rogers and R. G. Nuzzo, *Adv. Mater.*, 2005, **17**, 2332.
57 D.-Y. Khang, H. Jiang, Y. Huang and J. A. Rogers, *Science*, 2006, **311**, 208.
58 Y. Sun, V. Kumar, I. Adesida and J. A. Rogers, *Adv. Mater.*, 2006, **18**, 2857.
59 Y. Sun, W. M. Choi, H. Jiang, Y. Y. Huang and J. A. Rogers, *Nat. Nanotechnol.*, 2006, **1**, 201.
60 X. Chen and J. W. Hutchinson, *J. Appl. Mech.*, 2004, **71**, 597.
61 S. Wagner, S. P. Lacour, J. Jones, P.-H. I. Hsu, J. C. Sturm, T. Li and Z. Suo, *Physica E*, 2004, **25**, 326.
62 J. R. Morber, Y. Ding, M. S. Haluska, Y. Li, J. P. Liu, Z. L. Wang and R. L. Snyder, *J. Phys. Chem. B*, 2006, **110**, 21672.
63 J. Song, J. Zhou and Z. L. Wang, *Nano Lett.*, 2006, **6**, 1656.
64 A. Pan, H. Yamg, R. Liu, R. Yu, B. Zou and Z. Wang, *J. Am. Chem. Soc.*, 2005, **127**, 15692.
65 M. Law, D. J. Sirbuly, J. C. Johnson, J. Goldberger, R. J. Saykally and P. Yang, *Science*, 2004, **305**, 1269.
66 A. Maiti, J. A. Rodriguez, M. Law, P. Kung, J. R. McKinney and P. Yang, *Nano Lett.*, 2003, **3**, 1025.
67 J. S. Jie, W. J. Zhang, Y. Jiang and S. T. Lee, *Appl. Phys. Lett.*, 2006, **89**, 133118.
68 J. S. Jie, W. J. Zhang, Y. Jiang, X. M. Meng, Y. Q. Li and S. T. Lee, *Nano Lett.*, 2006, **6**, 1887.
69 Y. Jiang, W. J. Zhang, J. S. Jie, X. M. Meng, J. A. Zapien and S.-T. Lee, *Adv. Mater.*, 2006, **18**, 1527.
70 X. T. Zhou, F. Heigl, M. W. Murphy, T. K. Sham, T. Regier, I. Coulthard and R. I. R. Blyth, *Appl. Phys. Lett.*, 2006, **89**, 213109.
71 J. N. Lee, C. Park and G. M. Whitesides, *Anal. Chem.*, 2003, **75**, 6544.

